N93-27445

AN INTERACTIVE BOUNDARY-LAYER APPROACH TO MULTIELEMENT AIRFOILS AT HIGH LIFT

Tuncer Cebeci*
Aerospace Engineering Department
California State University, Long Beach

Abstract

A calculation method based on an interactive boundary-layer approach to multielement airfoils is described and is applied to three types of airfoil configurations with and without flap-wells in order to demonstrate the applicability of the method to general high-lift configurations. This method, well tested for single airfoils as a function of shape, angle of attack and Reynolds number, is here shown to apply equally well to two-element airfoils and their wakes, to a flap-well region, and to a three-element arrangement which includes the effects of co-flowing regions, a flap well, and the wake of the elements. In addition to providing accurate representation of these flows, the method is general so that its extension to three-dimensional arrangements is likely to provide a practical, accurate and efficient tool to assist the design process.

1.0 Introduction

The design of multielement airfoils for high lift requires consideration of a range of configurations so that care must be taken to ensure that the essential experiments and calculations can be undertaken with acceptable cost as well as accuracy.[1,2] We are concerned here with the development of a calculation method which meets this requirement and is able to represent the flow over and between the individual airfoils with consideration of flap wells and wakes. These requirements imply the need for a method which has an economical and accurate numerical solution procedure; a flexible turbulence model to represent wall boundary layers, wall jets and wakes, and the wake of the last element; and the ability to represent the separated flows associated with the upper surface and the flap well. In addition, the preferred procedure should be readily extendible to deal with three-dimensional components such as wings and empennage.

In recent years there has been a renewed interest in experimental work on high-lift systems. Extensive measurements have been reported by Nakayama[3], Alemdaroglu summarized by Nakayama[4], and Valarezo et al.[5] The data of Nakayama are for a three-element airfoil with a leading-edge slat and for a single-segment flap; they were obtained at NASA Langley's Low Turbulence Pressure Tunnel (LTPT). Those of Alemdaroglu are essentially for the same but smaller model and were obtained at the low-speed wind tunnel of California State University, Long Beach. The data of Valarezo et al. were also obtained at NASA Langley's LTPT and correspond to measurements at high Reynolds numbers. These data add to the previously obtained data on multielement airfoils by van den Berg,[6] van den Berg and Oskam[7], Oskam et al.[8], Omar et al.[9,10] and Olson and Orloff[11] which allow the validation of computer programs to analyze high-lift systems.

Several airfoil-analysis and design algorithms have been developed in the last decade and have been based on one of two approaches: numerical solutions of the Reynolds-averaged Navier-Stokes equations or solutions of the interaction between inviscid and boundary-layer equations. The former approach involves the numerical solution of elliptic equations so that information travels in all directions through pressure, velocity and viscous and turbulent stress gradients. As a result, the solution method requires simultaneous processing of the pressure and velocity components and stress tensor throughout the flowfield and this, in turn, implies a trade-off between accuracy and cost which tends to limit the validity of this approach. This limitation is a function of computers and programming methods, and these are likely to improve with time so that solutions of the Navier-Stokes equations, with proper consideration of momentum conservation in two directions together with longitudinal diffusion, are likely to be a major component of design methods of the future. The combination of the largest mainframe computers and unstructured and multigrid techniques has already been shown to be very powerful as, for example, by Mavriplis[12], Rogers et al.[13], and Barth.[14]

The present approach is based on the interactive boundary-layer approach which has been tested extensively for single-element airfoils, as described for example in References 15 to 17. These papers have shown that this approach can represent accurately, and with low cost, the flows around a number of airfoil geometries, with angles of attack up to and beyond that of stall, and including regions of separated flow which may cause transition from laminar flow. It is based on solutions of inviscid and boundary-layer equations with a surface and wake blowing velocity obtained from the Hilbert integral and ensuring interaction between the calculated inviscid and viscous flows. It has also been shown that, in extended form, it is able to represent the three-dimensional flows over wings[18] and, therefore, meets many of the requirements for a design method as discussed above.

It should be emphasized that alternative interactive methods have been reported, for example by Veldman[19], LeBalleur[20,21], Williams and Smith[22], Drela and Giles[23], and Kusunose, Wigton and Meredith.[24] The last of these deserves further research in the context of this paper since it has been reported recently and has been applied to multielement airfoils. It uses a finite-element full-potential code to compute the outer flow with a modified streamline H-grid, and solves the boundary-layer equations in integral form with modeling similar to that of Bradshaw and Ferris.[25]

*Professor and Chairman.

The results encompass single, two- and three-element airfoils at angles of attack up to around 13 degrees and are in close agreement with measurements. It is also evident that the method is cost efficient and is already part of a design method. It can be expected, however, that the turbulence model will be less successful where pressure gradients are severe and will not cope well with inter-element flows where there is a distinct velocity maximum. In addition, and perhaps of greatest importance, attempts to extend integral boundary-layer methods to three-dimensional flows have not been successful.

This paper is concerned with the extension of the interactive boundary-layer method of Refs. 15 to 17 to represent multielement airfoils where the flows between airfoils, flap wells and the possible influence of the overall wake in all elements are new features. The computational investigation was carried out in three parts which are reflected in the presentation of results and correspond to two-element airfoils with emphasis on the flow between elements and the wake, a single-element airfoil with a flap well where the calculation of the flow in the flap well is the major novelty, and the combination of these features in three-element airfoils which involve a flap well. This results section is preceded by descriptions of the interactive and solution procedures and followed by concluding remarks.

2.0 Interactive Boundary-Layer Method

The interactive boundary-layer method makes use of the panel method of Hess and Smith[26] and a solution of the boundary-layer equations in which the turbulence model is given by the algebraic eddy viscosity (ε_m) formulation of Cebeci and Smith.[27] With b denoting $1 + \varepsilon_m/\nu$, the continuity and momentum equations can be written as

$$\frac{\partial u}{\partial x} + \frac{\partial v}{\partial y} = 0 \tag{1}$$

$$u \frac{\partial u}{\partial x} + v \frac{\partial u}{\partial y} = u_e \frac{du_e}{dx} + \nu \frac{\partial}{\partial y}\left(b \frac{\partial u}{\partial y}\right) \tag{2}$$

In the absence of mass transfer, the boundary conditions for the above equations on the airfoil are:

$$u = v = 0, \qquad y = 0 \tag{3a}$$

$$u \to u_e(x), \qquad y \to \infty \tag{3b}$$

and in the wake, where a dividing line at $y = 0$ is required to separate the upper and lower parts of the inviscid flow and in the absence of the normal pressure gradient, they are:

$$y \to \pm\infty, \quad u \to u_e(x); \quad y = 0, \quad v = 0 \tag{4}$$

2.1 Interaction Law

To perform the calculations for flows with separation, it is necessary to use an inverse procedure and compute the external velocity as part of the solution. Here we use the formulation discussed in Ref. 15 and write the edge boundary condition as

$$u_e(x) = u_e^0(x) + \delta u_e(x) \tag{5a}$$

with $\delta u_e(x)$ computed from the Hilbert integral

$$\delta u_e(x) = \frac{1}{\pi} \int_{x_a}^{x_b} \frac{d}{d\sigma}(u_e \delta^*) \frac{d\sigma}{x - \sigma} \tag{5b}$$

This inverse boundary-layer formulation is appropriate to airfoils and to those parts of airfoils without surface discontinuities such as flap wells. Where flap wells occur, a different formulation of the inverse procedure is required, and the formulation used here is described below.

The calculation of the flow in the flap-well region is similar to that over a backward-facing step. A large portion of the flow separates immediately after the sudden change of the geometry, and the size of the reversed-flow region depends mainly on the step height, on the gap, and the overhang. The flow reattaches and gradually recovers downstream in the flap-well region or in the wake. The calculation of flows of this kind is difficult, and potential theory is not adequate because of the singularity that occurs at the geometry discontinuity and the strong viscous effects in the separated flowfield. Thus, an initial distribution of displacement thickness is assumed and the relaxation formula

$$(\delta^*)^{\nu+1} = (\delta^*)^{\nu}\left[1 + \omega\left(\frac{u_{ev}}{u_{ei}} - 1\right)\right] \tag{6}$$

is used in the inverse method to replace the Hilbert integral formulation of the external boundary condition. The new edge boundary conditions are given by Eq. (3b) and Eq. (6), where u_{ev} and u_{ei} correspond to the external velocities computed by the boundary layer and inviscid methods, respectively, and ω is a relaxation parameter. At the end of the flap-well region, the solution procedure reverts to the Hilbert-integral approach.

2.2 Turbulence Model

The turbulence model used to represent the flow on the airfoil may be expressed in terms of the Cebeci and Smith eddy-viscosity formulation,

$$\varepsilon_m = \begin{cases} (\varepsilon_m)_1 = \{0.4y[1 - \exp(\frac{-y}{A})]\}^2 \left|\frac{\partial u}{\partial y}\right| \gamma_{tr} \\ \qquad\qquad 0 \le y \le y_c \quad (7a) \\ (\varepsilon_m)_o = 0.0168 \left| \int_0^{\infty} (u_e - u)dy \right| \gamma_{tr}\gamma \\ \qquad\qquad y_c \le y \le \delta \quad (7b) \end{cases}$$

where

$$A = 26\nu u_\tau^{-1}, \quad u_\tau = \left(\frac{\tau}{\rho}\right)_{max}^{1/2}, \quad \gamma = \frac{1}{1 + 5.5(y/\delta)^6} \tag{8a}$$

The condition used to define y_c is the continuity of the eddy viscosity so that Eq. (7a) is applied from the wall outward (inner region) until its value is equal to that given for the outer region by Eq. (7b). The expression γ_{tr} represents the transition region and is given by

$$\gamma_{tr} = 1 - \exp[G(x - x_{tr}) \int_{x_{tr}}^{x} \frac{dx}{u_e}] \tag{8b}$$

Here x_{tr} is the location of the beginning of transition and G is defined by

$$G = \frac{1}{1200}\frac{u_e^3}{\nu^2} R_{x_{tr}}^{-1.34}$$

where the transition Reynolds number $R_{x_{tr}} = (u_e x/\nu)_{tr}$.

The location of the onset transition is obtained from Michel's formula, given by Ref. 28,

$$R_\theta = 1.174\left(1 + \frac{22{,}400}{R_x}\right) R_x^{0.46} \tag{9}$$

When flow separation takes place upstream of the transition location predicted by this formula, transition is assumed to coincide with the location of separation.

In the flap-well region, the above formulas are modified so that

$$\epsilon_m = \epsilon_m^{(I)} + (\epsilon_m^{(F)} - \epsilon_m^{(I)})(1 - e^{-(x-x_o)/\lambda L}) \tag{10}$$

Here $\epsilon_m^{(I)}$ denotes the eddy viscosity corresponding to the velocity profile above the separated region and $\epsilon_m^{(F)}$ includes the total region from the wall. The expressions for $\epsilon_m^{(I)}$ and $\epsilon_m^{(F)}$ are given by:

$$\epsilon_m^{(I)} = \begin{cases} \{0.4(y - y_o)[1 - e^{-(y-y_o)/A}]\}^2 \left|\frac{\partial u}{\partial y}\right|_{\Upsilon_{tr}} & \text{for } y > y_o \\ 0.0168\, u_e \left|\int_{y_o}^{\infty}(1 - \frac{u}{u_e})dy\right|_{\Upsilon\Upsilon_{tr}} & \text{for } y > y_o \\ 0 & \text{for } y < y_o \end{cases} \tag{11a}$$

$$\epsilon_m^{(F)} = \begin{cases} \{0.4y\,[1 - e^{-y/A}]\}^2 \left|\frac{\partial u}{\partial y}\right|_{\Upsilon_{tr}} & \text{for } y > 0 \\ 0.0168\, u_e \left|\int_{0}^{\infty}(1 - \frac{u}{u_e})dy\right|_{\Upsilon\Upsilon_{tr}} & \text{for } y > 0 \end{cases} \tag{11b}$$

where y_o is the location of $u = 0$, λ is a relaxation parameter (usually around 10), L is a characteristic length, and x_o is the beginning of the flap-well.

In the wake the corresponding expressions are:

$$\epsilon_m = (\epsilon_m)_w + [(\epsilon_m)_{t.e.} - (\epsilon_m)_w] \exp\left[\frac{(x - x_o)}{20\delta}\right] \tag{12}$$

where $(\epsilon_m)_{t.e.}$ is the eddy viscosity at the trailing edge computed from Eqs. (7) and (10) and $(\epsilon_m)_w$ is the eddy viscosity in the far wake given by the larger of

$$(\epsilon_m)_w^{\ell} = 0.064 \int_{-\infty}^{y_{min}} (u_e - u)dy \tag{13a}$$

and

$$(\epsilon_m)_w^{u} = 0.064 \int_{y_{min}}^{\infty} (u_e - u)dy \tag{14b}$$

with y_{min} denoting the location where the velocity is a minimum.

The eddy-viscosity model for the flap-well, like all expressions for turbulent flows, is empirical and was first tested for flow over a backward facing step before its application to the present problem. While the agreement with backward facing data was satisfactory, it should be tested further and possibly replaced by "better" expressions or models.

2.3 Solution Procedure

In general, it is convenient to solve the equations of the previous section in transformed variables. The Falkner-Skan transformation defined by

$$\eta = \left(\frac{u_e}{\nu x}\right)^{1/2} y, \quad \psi = (u_e \nu x)^{1/2} f(x,\eta) \tag{15}$$

is used here and, with the usual definition of stream function, Eqs. (1) - (3) lead to

$$(bf'')' + \frac{1}{2}(m + 1)ff'' + m(1 - f'^2) = x\left(f'\frac{\partial f'}{\partial x} - f''\frac{\partial f}{\partial x}\right) \tag{16}$$

$$\eta = 0, \quad f = f' = 0, \quad \eta = \eta_e, \quad f' = 1, \tag{17}$$

where primes denote differentiation with respect to η and

$$f' = \frac{u}{u_e}, \qquad m = \frac{x}{u_e}\frac{du_e}{dx}$$

A slightly modified form of this transformation is used when the calculations are performed in the inverse mode by replacing u_e with a reference velocity u_o, that is,

$$Y = \sqrt{u_o/\nu x}\, y, \quad \psi = \sqrt{u_o \nu x}\, F(x,Y) \tag{18}$$

so that the continuity and momentum equations and their boundary conditions, given by Eqs. (16) and (17) become,

$$(bF'')' + \frac{1}{2}FF'' + xw\frac{dw}{dx} = x\left[F'\frac{\partial F'}{\partial x} - F''\frac{\partial F}{\partial x}\right] \tag{19}$$

$$Y = 0, \qquad F = F' = 0 \tag{20a}$$

$$Y = Y_e, \qquad F' = w \tag{20b}$$

The boundary conditions corresponding to Eq. (5b) are obtained by applying a discretization approximation to the Hilbert integral, Eq. (5b),

$$u_e(x_i) = u_e^o(x_i) + c_{ii}D_i + \sum_{j=1}^{i-1} c_{ij}D_j + \sum_{j=i+1}^{N} c_{ij}D_j \tag{21}$$

where the subscript i denotes the x-station where the inverse calculations are to be performed, c_{ij} is a matrix of interaction coefficients, and D is given by $D = u_e\delta^*$. Further details are available in Ref. 15. In terms of transformed variables, the parameter D can be written as

$$D = \left(\frac{\nu x}{u_o}\right)^{1/2}(Y_e w - F_e) \tag{22}$$

and the relation between the external velocity w and displacement thickness δ^* provided by the Hilbert integral can then be written as

$$Y = Y_e, \qquad w = c_{11}\left(\frac{\nu x}{u_o}\right)^{1/2}(Y_e - F) + g_1 \quad (23)$$

where

$$g_1 = u_e^o(x_1) + \sum_{j=1}^{i-1} c_{1j}D_j + \sum_{j=i+1}^{N} c_{1j}D_j \quad (24)$$

In the flap-well region, Eq. (23) is replaced by

$$Y = Y_e, \qquad F_e = w[Y_e - \left(\frac{u_o}{\nu x}\right)^{1/2}\delta^*] \quad (25)$$

The corresponding boundary conditions in the wake are

$$Y = Y_{-e}, \quad F' = w; \quad Y = 0, \quad F = 0;$$

$$Y = Y_e, \quad F' = w,$$

with w now given by

$$w = c_{11}[w(Y_e - Y_{-e}) - (F_e - F_{-e})]\left(\frac{\nu x}{u_o}\right)^{1/2} + g_1, \quad (26)$$

The solution of the above transformed equations is obtained by Keller's box method, as described in Ref. 15. Where separation occurred, the convective term $u(\partial u/\partial x)$ was set to zero and this assumption proved to be satisfactory for the flow on the airfoil. The larger regions of separation associated with the flap well and the near wake required an additional iteration scheme based on a continuation method. Since a linearized form of the boundary-layer equations is being solved, it is necessary that the calculations at station x_i have initial profiles which are usually assumed to correspond to those at a previous x-station, x_{i-1}. With increasing flow separation, the effect of the initial profiles on the solutions at x_i increases and can lead to breakdown. A remedy to this problem is to define the velocity profile at x_i to be of the form

$$u = u_{ref} + n(u_a - u_{ref}) \quad (27)$$

where u_a denotes the velocity profile at x_{i-1} and u_{ref} to a profile which allows solutions to be obtained at x_i. The iteration process at x_i proceeds with values of n ranging from 0 to unity.

The sequence of the calculations is as follows. The panel method provides an external velocity distribution based on a body shape in which the flap-well region is assumed to be absent. The interactive boundary-layer approach leads to solutions on the upper surface from the stagnation point through the regions of laminar, transitional and turbulent flow to the trailing edge. Similarly, it provides results for the lower surface up to the beginning of the flap-well. A displacement thickness distribution, $\delta^*(x)$, is assumed in the flap well and, with the continuation method described above and with the initial velocity profile similar to that of a backward-facing step, calculations proceed to the trailing edge. With the upper and lower surface velocity profiles at the trailing edge, the calculations are extended into the wake. As a consequence of the above, a blowing velocity is available on the airfoil and in the wake. In the flap-well region, the blowing velocity v_n is defined by

$$v_n = \frac{d}{dx}(u_e\delta_m^*) \quad (28)$$

where $\delta_m^* = \delta^* - \delta_t$. Here δ_t corresponds to the body shape assumed to exist over the flap-well. Elsewhere, the blowing velocity is given by

$$v_n = \frac{d}{dx}(u_e\delta^*) \quad (29)$$

With the blowing velocity distribution known everywhere in the flowfield, a new distribution of external velocity $u_{e1}(x)$ is obtained from the panel method. As before, the boundary-layer solutions on the upper and lower surfaces of the airfoil are obtained with the Hilbert integral in which the edge boundary condition, Eq. (21), is now written as

$$u_e(x) = u_e^\kappa(x_1) + c_{11}D_1 + \sum_{j=1}^{i-1} c_{1j}(D_j - D_j^\kappa) + \sum_{j=i+1}^{N} c_{1j}(D_j - D_j^\kappa) - c_{11}D_1^\kappa \quad (30)$$

with κ indicating the iteration cycle. Equation (23) also changes to

$$g_1 = u_e^\kappa(x_1) + \sum_{j=1}^{i-1} c_{1j}(D_j - D_j^\kappa) + \sum_{j=i+1}^{N} c_{1j}(D_j - D_j^\kappa) - c_{11}D_1^\kappa \quad (31)$$

In the flap-well, with u_{ev} known from the previous flap-well calculation, a new δ^*-distribution is available from Eq. (6) and is used to obtain solutions up to the trailing edge. This sequence of calculations is repeated for the whole flowfield until convergence is achieved. The continuation method discussed before is involved within this sequence of calculations where necessary.

3.0 Results and Discussion

3.1 Two-Element Airfoil

In a previous study, a similar interactive approach was used to compute the performance characteristics of three two-element airfoils.[29] The inviscid flow solutions were obtained by the conformal-mapping method of Halsey[30], rather than the panel method used here, and the viscous-flow calculations were performed without accounting for the wake effects, either behind the main airfoil or the flap. The calculation method provided results which agreed well with experimental information within the accuracy of the measurements up to an angle of attack which was sufficiently small so that there was either no or very small separation on the airfoil and the gaps between the elements were comparatively large. In this way, the difficulties in computing the wake of each airfoil and accounting for the merging of the shear layers between the airfoil and the flap, and extending the range of the computational method to higher angles of attack were postponed to a later time.

In the studies reported here, we first performed calculations with the present method which did not include the wake effect and compared the results with those obtained with the earlier code[29] with its different inviscid flow method. After ensuring that the results of both codes were essentially the same, the wake effects were introduced into the present method and calculations were repeated for the three two-element airfoils to investigate the role of the wake effect on the solutions.

The first results of this paper are for two-element airfoils for which corresponding experimental investigations have been reported by Van den Berg[6], by Omar et al.[9,10] and Olson and Orloff.[11] There are no flap wells in these arrangements and the novel features of the calculations are the flow between elements and the inclusion of the wakes.

Figures 1-3 present the results of the data of Van den Berg[6], also discussed by Van den Berg and Oskam[7] and Oskam et al.[8], which correspond to a supercritical main airfoil (NLR 730) with a flap of 32% of the main chord at a deflection angle of 20 degrees. Measurements of surface pressure and velocity profiles were obtained a chord Reynolds number of 2.51×10^5 and for angles of attack of 6 and 13.1 degrees, the latter recognized as the highest angle which corresponded to fully attached flow. Lift coefficients were deduced for

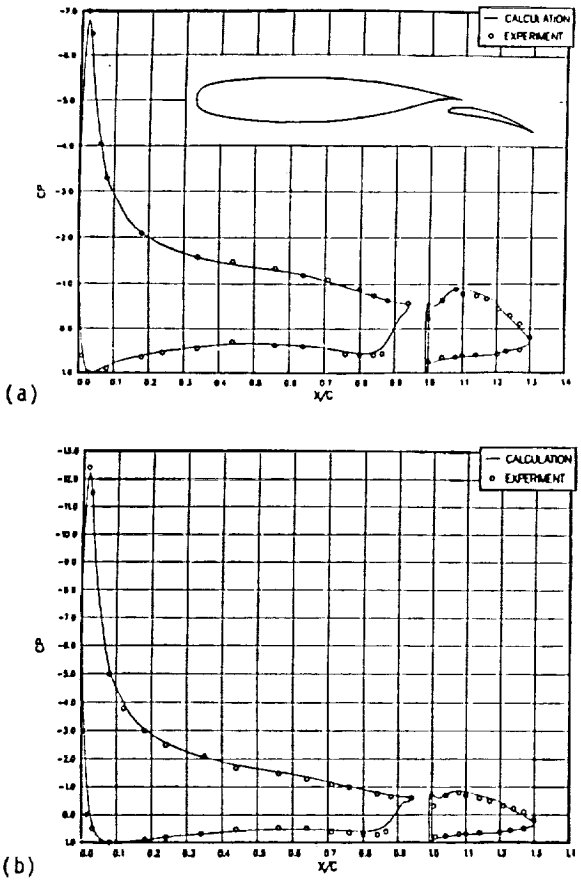

Fig. 1. NLR 7301 wing with flap. Calculated and measured: pressure distribution at (a) $\alpha = 6°$, (b) $\alpha = 13.1°$.

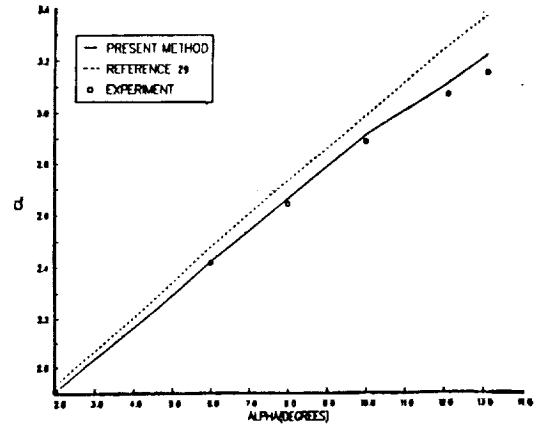

Fig. 2. NLR 7301 wing with flap. Calculated and measured lift coefficients.

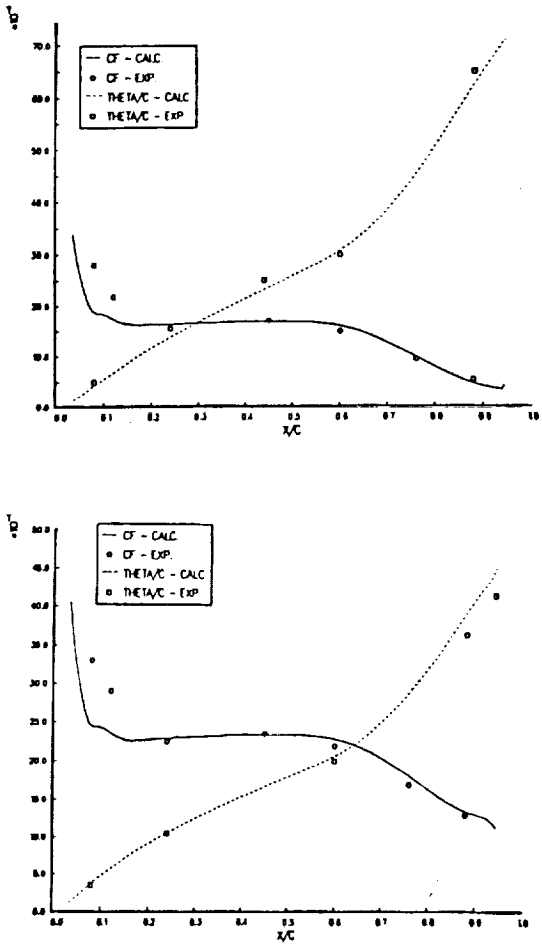

Fig. 3. NLR 7301 wing with flap. Calculated and measured: local skin-friction coefficients, c_f, and momentum thicknesses, θ/c, on the upper wing surfaces at (a) $\alpha = 6°$, (b) $\alpha = 13.1°$.

five angles of attack. The airfoil arrangement is shown on Fig. 1a and it is evident that the distributions of pressure coefficients are in close agreement with the measured values over the surfaces of both elements. The results at the angle of attack of 13.1 degrees confirm the absence of separation and the lift coefficients of Fig. 2 that stall occur at an angle larger than this

value. The calculated variation of lift coefficient with angle of attack is close to the measurement and some 3% lower than that calculated without consideration of the wake. It is to be expected that this difference will increase with angle of attack and particularly as separation occurs and expands over the upper trailing-edge region, and this trend is evident in the figure.

Figures 3a and 3b show the variations of momentum thickness and skin-friction coefficient with chord distance over the main airfoil. The agreement between calculated and measured results is remarkable for both angles of attack, the only significant discrepancies being in the skin-friction coefficient in the upstream region of maximum rate of change. Again, the results at 13.1 degrees confirm the absence of separation, although this result conveys little about the flow on the second element.

Figure 4 presents the results for a NASA supercritical airfoil, 24" in length, with a 7" flap at a deflection angle of 20 degrees. The experiments were carried out in the 36 x 96 in. wind tunnel of the Boeing Research Laboratories at a Mach number of 0.2 and have been documented by Omar et al.[9,10] The pressure-coefficient distributions of Figs. 4a and 4b correspond to angles of attack of zero and

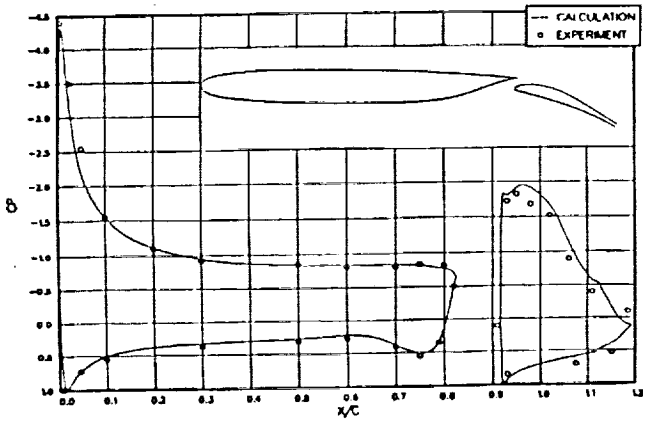

(a)

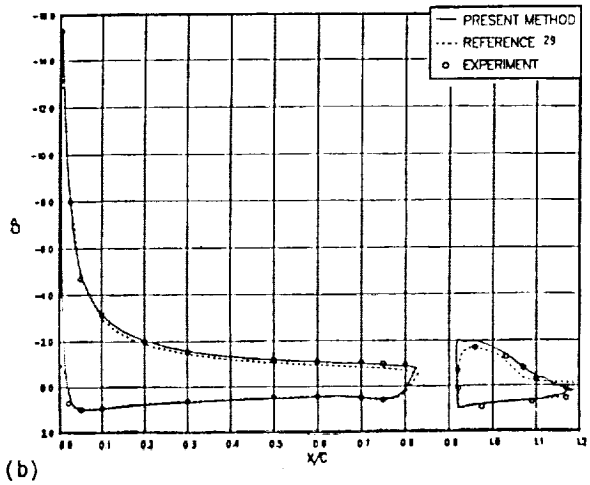

(b)

Fig. 4. NASA supercritical two-element airfoil. Calculated and measured: (a) pressure distribution at $\alpha = 0°$, (b) pressure distribution at $\alpha = 8.93°$, The results of Ref. 29 are without wake effect.

8.93 degrees with the measured and calculated values again within experimental uncertainty. The wake had no effect at zero angle of attack, as expected, and had a slight effect on the pressure coefficients at the 8.93 degree angle, although the improvement on the main airfoil is coupled with an apparent lack of improvement on the flap. These results are reflected in the lift coefficients of Fig. 5 where the calculated results with the wake effect are in better agreement with data than those without the wake effect.

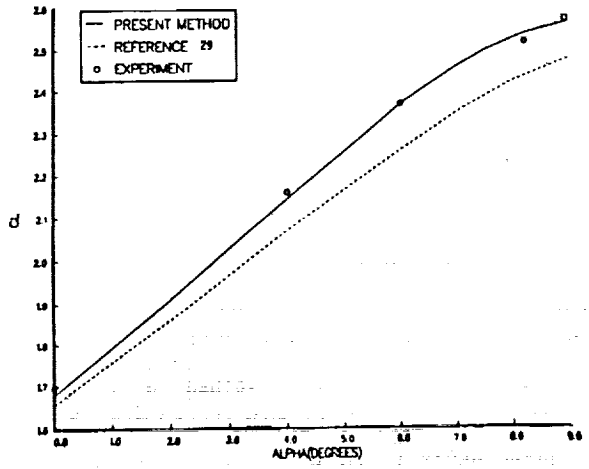

Fig. 5. NASA supercritical two-elemen' airfoil. Calculated and measured lift coefficients. The results of Ref. 29 are without wake effect.

The third two-element airfoil corresponds to that investigated by Olson and Orloff[11] which involves a NACA 4412 airfoil with a chord length of 0.9m upstream of a flap which has the section of a NACA 4415 airfoil and a chord of 0.36m with a deflection angle of 10°. Figure 6 shows the measured and calculated surface pressure distributions for a Reynolds number of 1.3×10^6 at an angle of attack of 2.2°. As in the first case, there is a slight improvement over the results obtained without the wake which, again, may be due to the absence of flow separation.

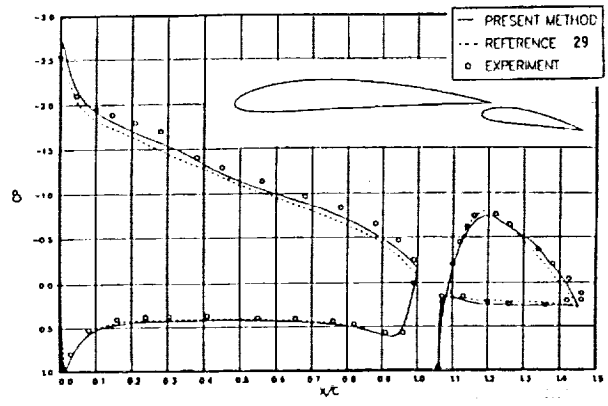

Fig. 6. NACA 4412/4415 airfoil. Calculated and measured pressure distributions for $\alpha = 2.2°$.

It is evident from the comparisons of Figs. 1-6 that the flow between the airfoil elements and the wake have been satisfactorily incorporated in the interactive procedure with results which are virtually identical to the measurements. It should, however, be noted that the effect of merging of the

boundary layers in these three configurations is negligible.

3.2 Single Airfoil with a Flap-Well

An appraisal of the interactive boundary-layer procedure, as applied to the flow in and around a flap well, required corresponding measurements and a parallel experimental program which was carried out at the California State University, Long Beach, with the single airfoil arrangement of Fig. 7. The experiment described in Ref. 4 used this 12-inch chord airfoil, which corresponds to the main element of the three-element configuration tested in the low-turbulence tunnel of the NASA Langley Research Center, and described by Nakayama.[3] The chord Reynolds number was 0.5×10^6, and surface pressures were measured for angles of attack up to 14 degrees with local velocity information in the flap well at an angle of attack of 5 degrees. Figure 8 presents the measured and calculated surface-pressure distributions for angles of attack of 5, 8 and 12 degrees with transition tripped at 0.25c, and the agreement is generally good. The calculated upper-surface pressure peak close to the leading edge reflects the better spatial resolution of the interactive method, and close to the trailing edge there are some small disagreements which may stem from the flap-well results. Nevertheless, the pressure-coefficient distributions represent closely the measurements in the flap-well with the near constant values indicating the region of recirculation followed, as can be seen, by a rapid increase in pressure coefficient after reattachment.

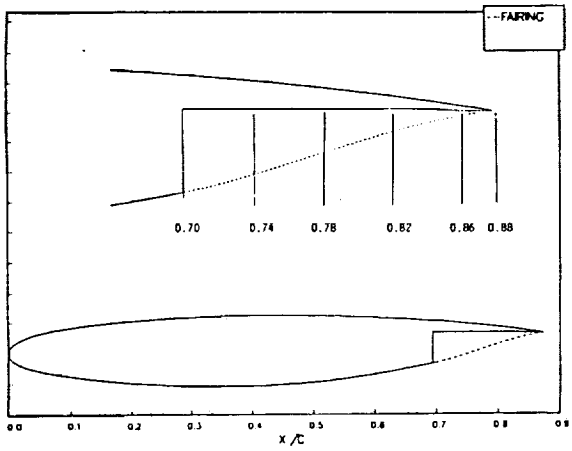

Fig. 7. Single airfoil with flap-well cut.

Figure 9 shows calculated profiles of streamwise velocity, streamlines and the distribution of skin-friction coefficients within the flap well. The profiles differ increasingly from the measurements in the near-wall region, although reattachment occurs at about the same location. The reasons for the discrepancy are likely to be associated with the turbulence model that is used here to represent a near-wall flow, which undoubtedly involves low-Reynolds-number characteristics together with a switch from a wall jet in the negative to a boundary layer in the positive direction. It is unlikely that these local differences will affect greatly the outer region, particularly since the negative velocities and momentum are small, so that the calculated distribution of displacement thickness of Fig. 9b is likely to be correct. The

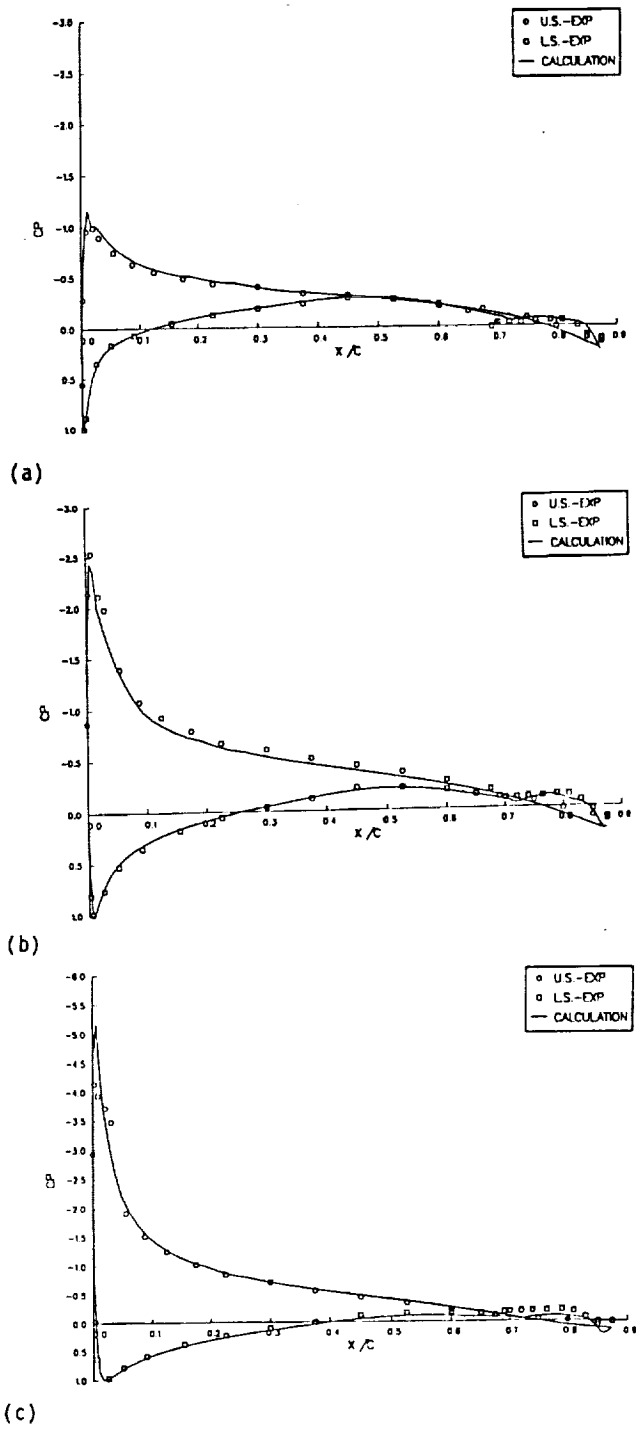

Fig. 8. Comparison of calculated pressure distributions with data for $R_c = 0.5 \times 10^6$ at (a) $\alpha = 5.0$, (b) $\alpha = 8.0$, (c) $\alpha = 12.0$.

distribution of skin-friction coefficient, Fig. 9c, indicates negative values up to reattachment at 0.87c which is in agreement with the velocity profiles.

3.3 Three-Element Airfoils

With the positive results of Figs. 1 to 9 for three two-element airfoils and for an airfoil with a flap-well, it is appropriate to consider the application of the interactive boundary-layer method to a three-element airfoil with a flap well.

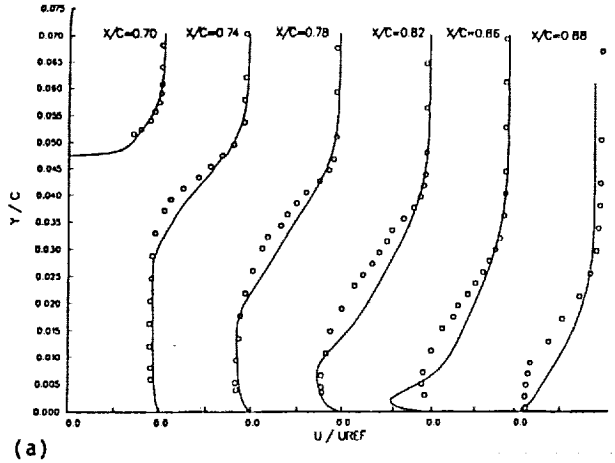

(a)

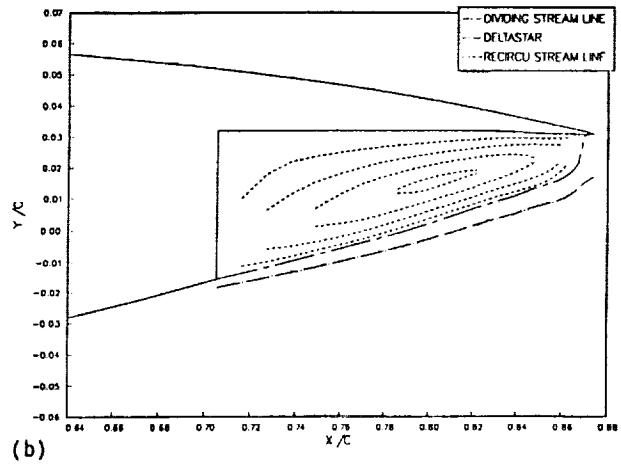

(b)

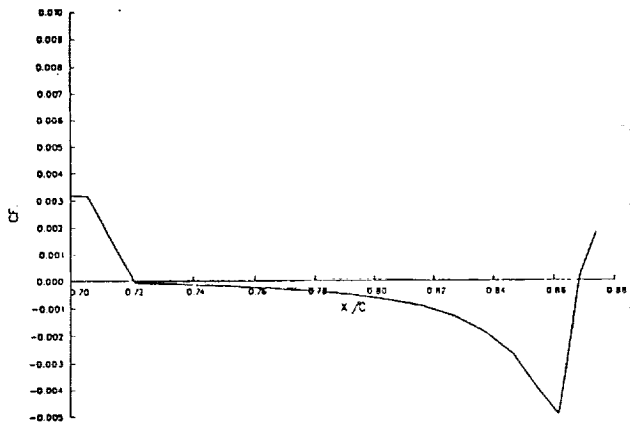

(c)

Fig. 9. Results for $R_c = 0.5 \times 10^6$ at $\alpha = 5.0$. (a) Velocity profiles in the flap-well region. (b) Recirculation streamline and the location of the displacement thickness. (c) Calculated local skin-friction coefficient in the flap-well region.

The chosen configuration is shown on Fig. 10 and corresponds to the high-lift model, tested in the NASA, Langley and California State wind tunnels at Reynolds numbers of 5×10^6 and 0.5×10^6, respectively.[3,4] The slat deflection angle was -30 degrees and the flap deflection angles 15 and 30 degrees with angles of attack of 4 to 20 degrees. The measurements were made by a combination of hot-wire and laser-velocimetry techniques, the latter was primarily used in regions of separated flow.

Fig. 10. The three-element airfoil with analytical and experimental fairing, $\delta_s = -30°$, $\delta_f = 15°$.

Calculations were initially made on smooth bodies without explicitly considering the flow in the flap-well region. Also, because the potential flow theory predicts flow singularities at the discontinuity of the airfoil geometry, the sharp corner of the slat and the flap-well cut out of the main airfoil were smoothed to prevent solutions from breaking. Figure 10 shows the modified geometry of this airfoil with the flap-well fairing and the rounded slat used in calculations. The so-called "experimental fairing" refers to the dividing streamline which was determined from measurements, while the "analytical fairing" was drawn arbitrarily. Figure 11 shows the velocity vectors for a particular combination of gap and overhang and the position of the streamline dividing the recirculating flow behind the flap-well step from the outside flow, as determined from the mean-velocity vector data. The position of this dividing streamline is important since it corresponds roughly to the equivalent smooth body with pressure distribution close to the real one. Hence, this dividing streamline was used as the "experimental fairing" in the calculations. Figure 12 shows the surface-pressure distributions on the slat, main airfoil, and flap at three angles of attack (4°, 12° and 16°) for the configuration with the experimental fairing, and Fig. 13 shows the corresponding distributions at the same angles of attack for the configuration with analytical fairing. Overall, the calculated results agree well with experimental data except for the slat at low angles of attack and the pressure peak on the main airfoil. This discrepancy may be caused by the differences between the assumed slat shape and the real one. In the flap-well region, the results are in better agreement with measurements when the fairing is close to a real streamline.

Finally, the method of Section 4.2 was applied to include the calculation inside the flap-well. The results, shown in Fig. 14, agree well with measurements for all the cases indicated above and including angles of attack up to 20°. This confirms that it is unnecessary to make a priori

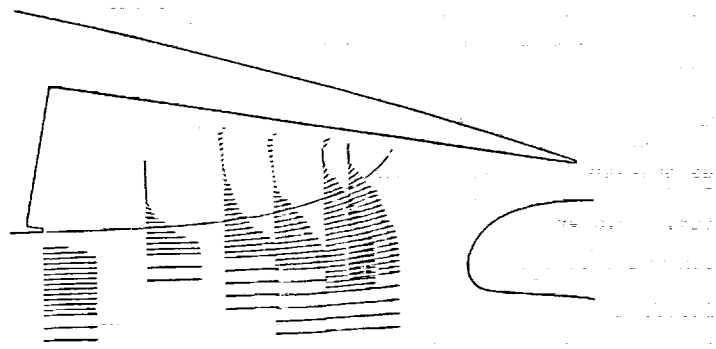

Fig. 11. Velocity vectors in the flap-well region by laser velocimeter.

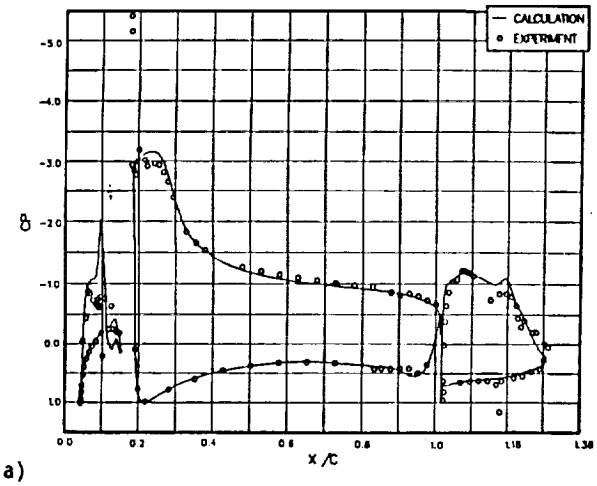

(a)

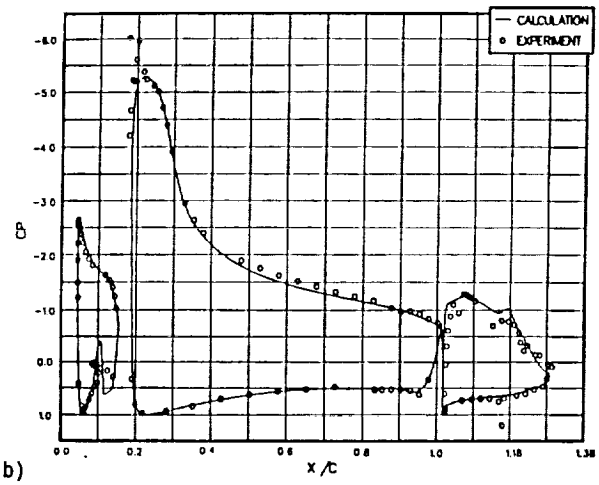

(b)

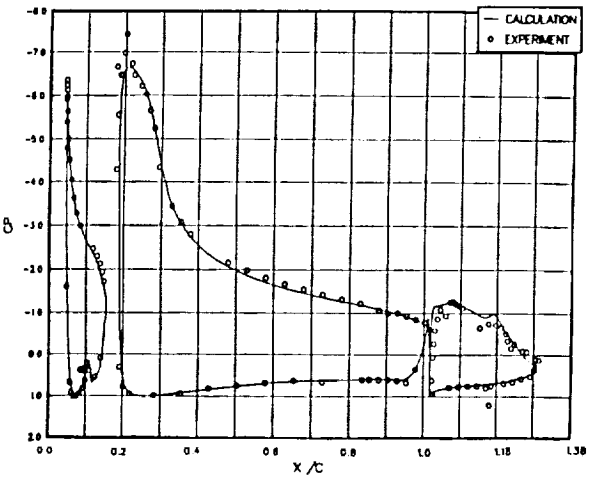

(c)

Fig. 12. Pressure distribution on the three-element airfoil with experimental fairing for δ_f = 15° and R_c = 5 x 10^6, (a) α = 4°, (b) α = 12°, (c) α = 16°.

assumptions about the fairing shape, and allows for further detailed investigations of the recirculation flow in the flap-well, such as the gap and overhang effects. Figure 15 shows the variation of lift coefficient with angle of attack, confirming that the present calculation method leads to values which are in close agreement with experiment.

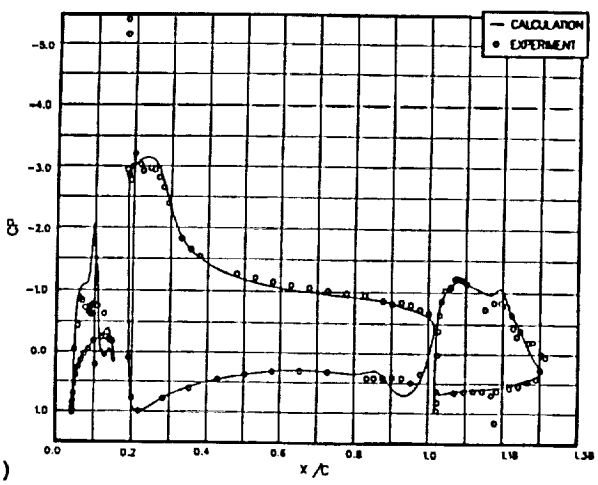

(a)

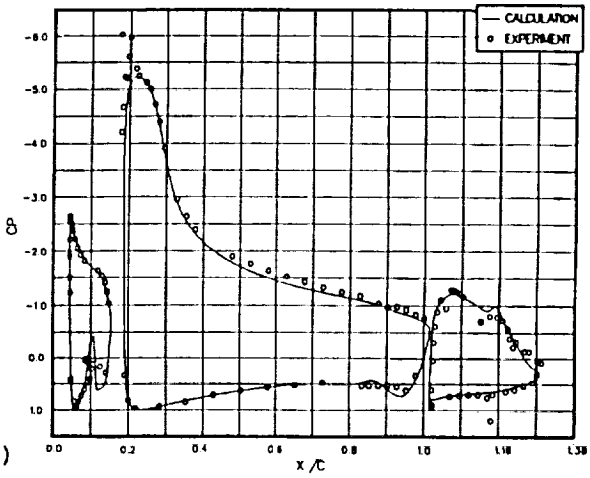

(b)

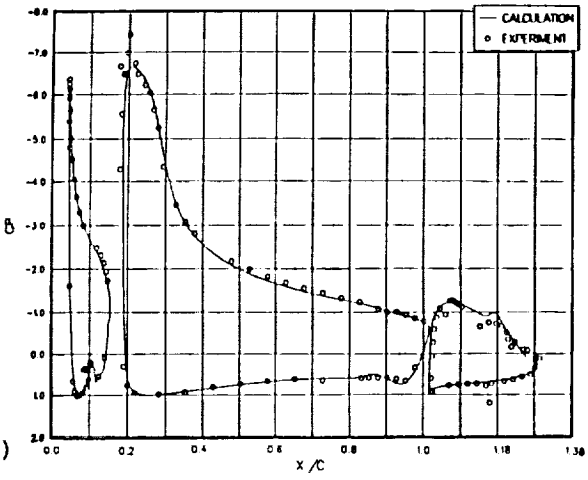

(c)

Fig. 13. Pressure distribution on the three-element airfoil with analytical fairing for δ_f = 15° and R_c = 5 x 10^6, (a) α = 4°, (b) α = 12°, (c) α = 16°.

Comparison of pressure coefficients for a flap deflection angle of 30°, Fig. 16, allows similar conclusions to be drawn to those of the previous paragraph. Also, the calculated lift coefficients shown in Fig. 17 are very close to measurements.

4.0 Concluding Remarks

The results and discussion of the previous section show that the present interactive method, with its consideration of the flap-well region and

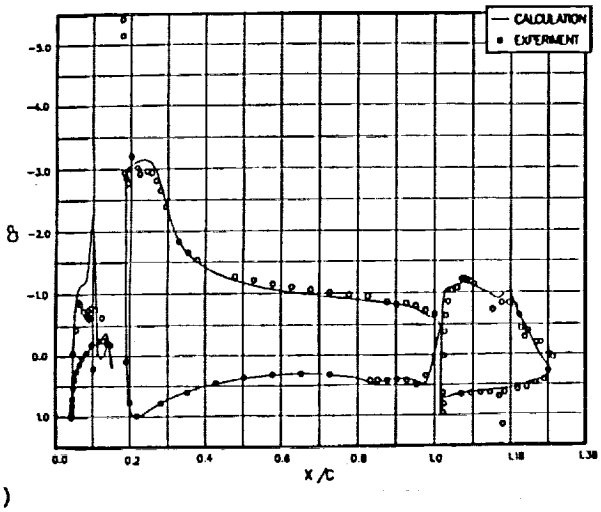

(a)

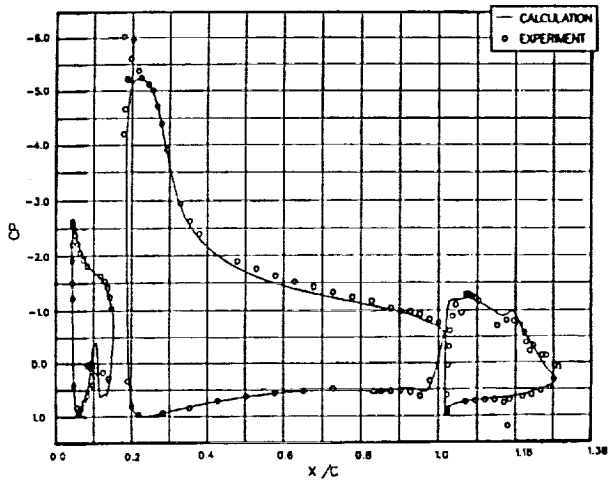

(b)

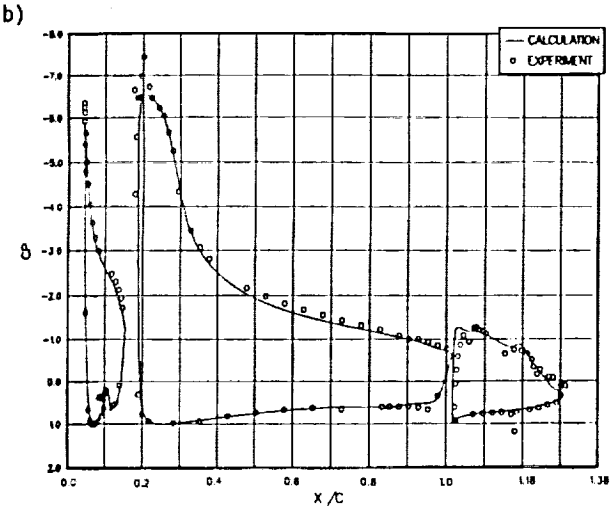

(c)

Fig. 14. Calculated and measured pressure distributions on the three-element airfoil for δ_f = 15° and R_c = 5 x 10^6 at (a) α = 4°, (b) α = 12°, (c) α = 16°, (d) α = 20°.

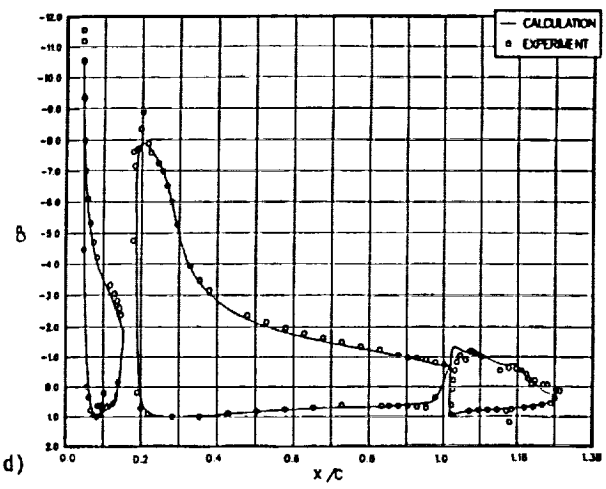

(d)

Fig. 14. Continued.

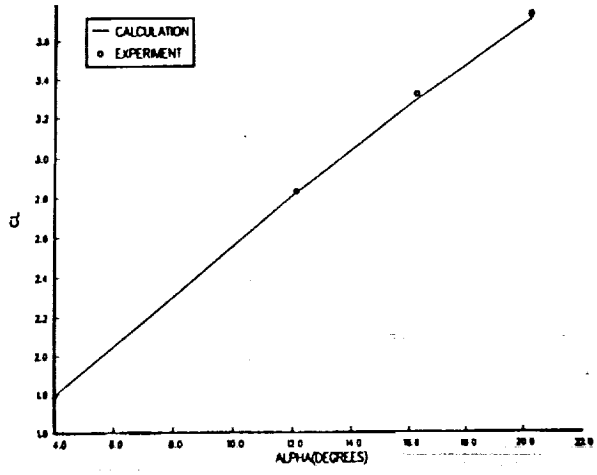

Fig. 15. Variation of the lift coefficient with angle of attack for the three-element airfoil with δ_f = 15° and R_c = 5 x 1^6.

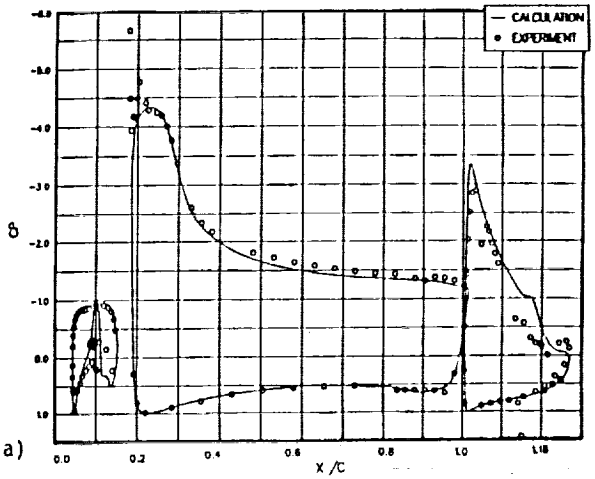

(a)

Fig. 16. Calculated and measured pressure distributions on the three-element airfoil with δ_f = 30° and R_c = 5 x 10^6, (a) α = 5°, (b) α = 15°, (c) α = 18°, (d) α = 20°.

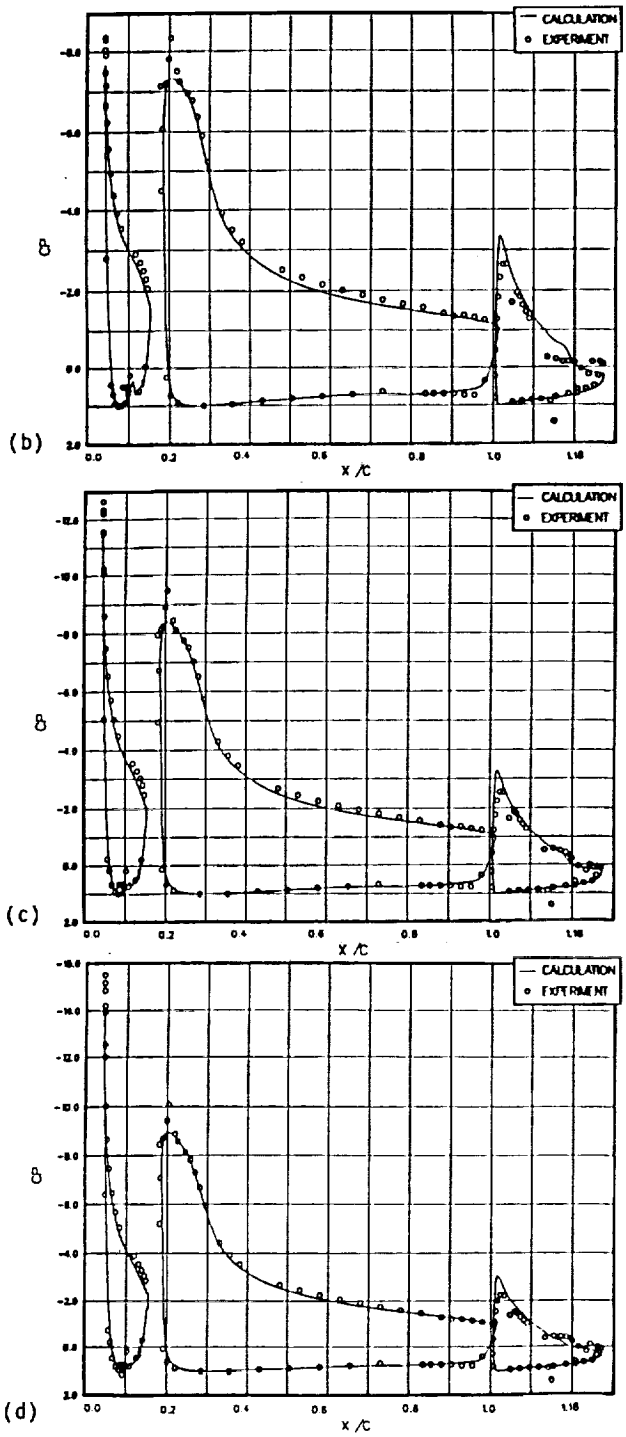

Fig. 16. Continued.

the wakes, leads to pressure coefficient distributions and values of lift which are in good agreement with experiment for single and multielement configurations with angles of attack up to 20°.

The present method neglects the confluent boundary layers, which become important as the distance between the main airfoil and the flap becomes smaller or where the shear layer thickens with angle of attack. Also, close examination of the turbulence model in the vicinity of this merging region is desirable. The incorporation of improvements to consider these aspects is likely to lead to a more generally applicable method.

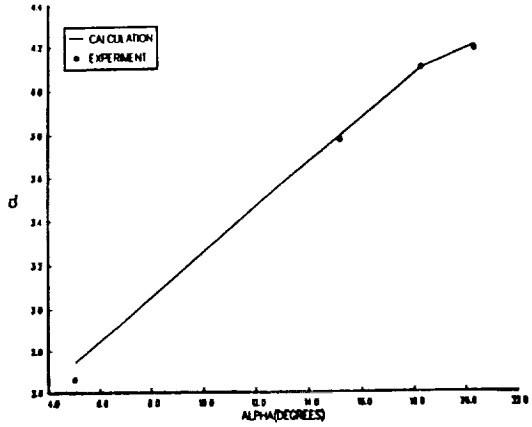

Fig. 17. Variation of the lift coefficient with angle of attack for the three-element airfoil with $\delta_f = 30°$ and $R_c = 5 \times 10^6$.

5.0 References

1. Smith, A.M.O., "High-Lift Aerodynamics," AIAA Paper No. 74-939, Aug. 1974

2. Garner, P.L., Meredith, P.T. and Stoner, R.C., "Areas for Future CFD Development as Illustrated by Transport Aircraft Applications," AIAA Paper No. 91-1527, 1991.

3. Nakayama, A., "Flowfield Survey Around High-Lift Airfoil Model LB 546," McDonnell Douglas Co. Report MDC J4827, 1987.

4. Nakayama, A., "An Experimental Investigation of a Flow Around the Flap Well of a Multi-element Airfoil," Douglas Aircraft Co. Report MDC K4310, 1990.

5. Valarezo, W.O., Dominik, C.J. and Wilcox, P.A., "High Reynolds Number Test Results for a Supercritical Multielement Airfoil," McDonnell Douglas Report No. MDC K5545, Dec. 1990.

6. Van den Berg, B., "Boundary-Layer Measurements on a Two-Dimensional Wing with Flap," NLR TR 79009U, 1979.

7. Van den Berg, B. and Oskam, B., "Boundary-Layer Measurements on a Two-Dimensional Wing with Flap and a Comparison with Calculations," Paper 18 of AGARD CP-271, 1979.

8. Oskam, B., Hahn, D.J. and Volkers, D.F., "Recent Advances in Computational Methods to Solve the High-Lift Multicomponent Airfoil Problem," NLR Report MP84042U, 1984.

9. Omar, E., Zierten, T. and Mahal, A., "Two-Dimensional Wind-Tunnel Tests of a NASA Supercritical Airfoil with Various High-Lift Systems. 1 - Data Analysis," NASA CR-2214, 1973.

10. Omar, E., Zierten, T., Hahn, M., Szpiro, E. and Mahal, A., "Two-Dimensional Wind-Tunnel Tests of a NASA Supercritical Airfoil with Various High-Lift Systems. 2 - Test Data," NASA CR-2215, 1977.

11. Olson, L. and Orloff, K.L., "On the Structure of Turbulent Wakes and Merging Shear Layers of Multielement Airfoils," AIAA paper 81-1238, June 1981.

12. Mavriplis, D.J., "Research on Unstructured Grid Techniques for CFD at ICASE," Paper presented at the CFD Conference, NASA Ames, 12-14 March 1991.

13. Rogers, E.S., Wiltberger, N.L. and Kwak, D., "Efficient Simulation of Incompressible Viscous Flow Over Single and Multielement Airfoils," AIAA Paper No. 92-0405.

14. Barth, T.J., "CFD Algorithms on Unstructures Meshes," Paper presented at the CFD Conference, NASA Ames, 12-14 March 1991.

15. Cebeci, T., Clark, R.W., Chang,, K.C., Halsey, N.D. and Lee, K., "Airfoils with Separation and the Resulting Wakes," Journal Fluid Mechanics, Vol. 153, pp. 323-347, 1986.

16. Cebeci, T., Jau, J., Vitiello, D. and Chang, K.C., "Prediction of Post-Stall Flows on Airfoils," in Numerical and Physical Aspects of Aerodynamic Flows, IV, (ed. T. Cebeci) Springer-Verlag, Heidelberg, 1990.

17. Cebeci, T., "Essential Ingredients of a Method for Low Reynolds-Number Airfoils," AIAA Journal, Vol. 27, pp. 1680-1688, 1983.

18. Cebeci, T., Khattab, A.A., Chen, H.H. and Chen, L.T., "An Approach to the Design of Wings: The Role of Mathematics, Physics and Economics," AIAA Paper 92-0286, 1992.

19. Veldman, A.E.P., Lindhout, J.P.F., deBoer, E., Somers, M.A.M., "VISTRAFS: A Simulation Method for Strongly Interacting Viscous Transonic Flow," in Numerical and Physical Aspects of Aerodynamic Flows, IV, (ed. T. Cebeci) Springer-Verlag, Heidelberg, 1990.

20. LeBalleur, J.C., "Couplage Visqueux-Non Visqueux: Methods Numerique et Applications Aux Ecoulements Bidimensionnels Transsoniques et Supersonicques," La Recherche Aerospatiale, Mar-Apr 1978.

21. LeBalleur, J.C., "New Possibilities of Viscous-Inviscid Numerical Techniques for Solving Viscous Flow Equations with Massive Separation," in Numerical and Physical Aspects of Aerodynamic Flows, IV, (ed. T. Cebeci) Springer-Verlag, Heidelberg, 1990.

22. Williams, B.R. and Smith, P.D., "Coupling Procedures for Viscous-Inviscid Interaction for Attached and Separated Flows on Swept and Tapered Wings," in Numerical and Physical Aspects of Aerodynamic Flows, IV, (ed. T. Cebeci), pp. 53-70, Springer-Verlag, Heidelberg, 1990.

23. Drela, M. and Giles, M.B., "Viscous-Inviscid Analysis of Transonic and Low Reynolds Number Airfoils," AIAA Journal, Vol. 25, 1987.

24. Kusunose, K., Wigton, L. and Meredith, P., "A Rapidly Converging Viscous/Inviscid Coupling Code for Multielement Airfoil Configurations" AIAA Paper 91-0177, 1991.

25. Bradshaw, P. and Ferris, D.H., "Calculations of Boundary-Layer Development Using Turbulent Energy Equation: Compressible Flow on Adiabatic Walls," Journal Fluid Mechanics, Vol. 46, 1970.

26. Hess, J.L. and Smith, A.M.O., "Calculation of Potential Flow About Arbitrary Bodies." Progress in Aerospace Sciences, Vol. 8, Pergamon Press, New York, 1966.

27. Cebeci, T. and Smith, A.M.O., Analysis of Turbulent Boundary Layers, Academic Press, New York, 1974.

28. Cebeci, T. and Bradshaw, P., Physical and Computational Aspects of Convective Heat Transfer, Springer-Verlag, N.Y., 1988.

29. Cebeci, T., Chang, K.C., Clark, R.W. and Halsey, N.D., "Calculation of Flow Over Multielement Airfoils at High Lift," Journal of Aircraft, Vol. 14, pp. 546-551, 1987.

30. Halsey, N.D., "Potential Flow Analysis of Multielement Airfoils Using Conformal Mapping," AIAA Journal, Vol. 17, p. 1281, 1979.

0750c